Quantum Information Processing (2019) 18:68
https://doi.org/10.1007/s11128-019-2183-z

Designs of interactions between discrete- and continuous-variable states for generation of hybrid entanglement

Sergey A. Podoshvedov[1] · **Nguyen Ba An**[2,3]

Received: 13 August 2018 / Accepted: 12 January 2019

Abstract
We develop theory of realizing different types of hybrid entanglement between discrete-variable (single photon) and continuous-variable states (coherent states). The key mechanism for generating such hybrid entangled states is thanks to superposing microscopic discrete-variable state with macroscopic continuous-variable Schrodinger cat state on highly transmissive beam splitter followed by measurement strategies in such a way that all the information about the amplitude of the continuous-variable state is erased. Conditions for obtaining the balanced hybrid entangled states are established and their degree of entanglement is evaluated.

Keywords Displaced number states · DV–CV interaction · Schrodinger cat state

1 Introduction

In optical quantum information processing, there are two different approaches described in discrete-variable (DV) [1] and continuous-variable (CV) [2] frameworks. The approaches use one of the aspects of the particle–wave duality [3]. Many protocols employ the particle-like discrete nature of light (e.g., superposition of vacuum and single photon $a_0|0\rangle + a_1|1\rangle$ or superposition of horizontally and vertically polarized

✉ Sergey A. Podoshvedov
sapodo68@gmail.com

Nguyen Ba An
nban@iop.vast.ac.vn

1 Department of Computer Modeling and Nanotechnology, Institute of Natural and Exact Sciences, South Ural State University (SUSU), Lenin Av. 76, Chelyabinsk, Russia

2 Thang Long Institute of Mathematics and Applied Sciences (TIMAS), Thang Long University, Nghiem Xuan Yem, Hoang Mai, Hanoi, Vietnam

3 Institute of Physics, Vietnam Academy of Science and Technology (VAST), 18 Hoang Quoc Viet, Cau Giay, Hanoi, Vietnam

Published online: 24 January 2019

photons $a_0|H\rangle + a_1|V\rangle$) to encode quantum information. Maximally entangled states from four-dimensional Hilbert space are required to implement quantum protocols with such DV states. Alternatively, the CV approach employs states which are determined in infinite-dimensional space such as coherent states $|\pm\alpha\rangle$ or Schrodinger cat states $a_0|-\alpha\rangle \pm a_1|\alpha\rangle$ with macroscopic continuous amplitudes $\pm\alpha$ [4]. Each approach has its own inherent advantages and drawbacks [5–10]. The Bell measurement is the main ingredient of quantum teleportation and construction of two-qubit controlled-X operation [5], so its practical implementation is one of the major problems in quantum information processing. Since only two of four Bell states can be discriminated by linear optics and photodetection [6], the protocols succeed only with 50% [7, 8] or even 25% probability [9], respectively. Theoretical schemes proposed in [1] can hardly be realized at least at the current level of technological development. As for the CV approach, an entangled resource can be provided, say, by a two-mode squeezed state [2], but CV teleportation fidelity cannot be deterministic because CV resources are not maximally entangled [10]. Recently, generation of multi-photon states entangled in their dual wave–particle natures as well as possibility of continuous transitions back and forth between wave-like and particle-like behavior are theoretically proposed [11, 12] and experimentally demonstrated [12]. Such refined manifestation of the wave—particle duality promises potential applications by encoding information in terms of the wave–particle degrees of freedom.

In the optical domain, coherent states as macroscopic states of light are most suited in the CV framework, while single-photon states as microscopic ones are the best candidates in the DV framework. A state that incorporates both DV and CV components is called hybrid. Realization of hybrid entanglement is of great interest for some reasons. On one side, it may answer fundamental questions underlying principles of the separation between the classical and quantum worlds, for example, the question concerning the so-called Schrödinger cat paradox [13] where macroscopic classical states are entangled with microscopic quantum ones. On the other side, combining both approaches to realize hybrid architecture may overcome the current limitations [14–17]. Experimental aspects of generation of various hybrid entangled states have been a subject of intense research [18–20]. Different types of optical arrangements have been proposed for the generation. General features of the hybrid DC–CV entanglement that could be exploited for advanced quantum optical technologies are analyzed in [21], relying on various manifestations of the photon subtraction technique by recording a certain measurement outcome in an auxiliary mode. All the above-mentioned protocols exploit the interaction between CV states in infinite-dimensional Hilbert spaces and DV states in finite-dimensional Hilbert spaces. But, of interest are also hybrid entangled DV states living in Hilbert spaces with arbitrarily different dimensions [22].

Here, we study a more general mechanism for generating DV–CV entanglements using peculiarities of interaction between DV and CV states (DV–CV interaction). The mechanism relies on indistinguishably displacing DV state in the phase space at the same time by equal-in-magnitude but opposite-in-sign macroscopic displacement vectors. Such operation can be done by mixing the DV state of interest with big-size Schrodinger cat by means of highly transmissive beam splitter (HTBS) [23–25]. The displacement should be performed in such a way that all information about the amount by which the interested DV state is displaced in the phase space is totally erased. Such

information erasing is achieved by counting photon number in the auxiliary output modes heralding generation of the desired hybrid state. The feature of the DV–CV interaction on a HTBS rests in the fact that the sign of the amplitude of the displaced state in the measurement carried out in the number state basis changes when the displacement vector changes its sign [26–28]. It is related to action of the controlled-Z gate on the DV qubit. This method proves to be universal allowing us to realize different types of hybrid states. In particular, in this work we are concerned with generation of two types of hybrid entangled states. The first type consists of coherent components and single-rail qubit composed of the vacuum state and the single-photon state. The second type is in terms of dual-rail photonic qubit. The generation schemes for the two types of hybrid entangled states differ by an additional procedure of the displacement in the auxiliary mode. We also establish the conditions to obtain the balanced hybrid states whose degree of entanglement is evaluated by means of relevant entanglement measures. The effectiveness of our entanglement generation schemes in terms of the success probability and the fidelity is considered as well.

2 DV–CV interactions

2.1 Hybrid entanglement between a CV and a single-rail DV states

Consider a typical optical device, the beam splitter (BS), which is described by the following unitary matrix

$$BS = \begin{bmatrix} t & -r \\ r & t \end{bmatrix}, \tag{1}$$

where t and r are, respectively, the transmittance and reflectance coefficients, satisfying the normalization condition $t^2 + r^2 = 1$. The action of the BS on two coherent states $|\alpha\rangle_1|\beta\rangle_2$ with α and β the corresponding amplitudes, which are assumed for simplicity to be real and positive, reads

$$BS|\alpha\rangle_1|\beta\rangle_2 = |\alpha t + \beta r\rangle_1|\beta t - \alpha r\rangle_2. \tag{2}$$

In a particular case, in which $t \approx 1$ (i.e., $r \approx 0$), $\beta \gg 1$ and ρ an arbitrary state one has [29]

$$BS(\rho \otimes |\beta\rangle\langle\beta|)BS^{+} \approx D(\alpha)\rho D^{+}(\alpha) \otimes |\beta\rangle\langle\beta|, \tag{3}$$

with

$$\alpha = \beta r \tag{4}$$

in the limit case of $t = 1$. In (3), $D(\alpha)$ is the displacement operator whose definition is given by (A1) in "Appendix A", where α is displacement amplitude, the symbol $\otimes$ means tensor product and $D^{+}(\alpha)$ is Hermitian conjugate of $D(\alpha)$. The action of $D(\alpha)$

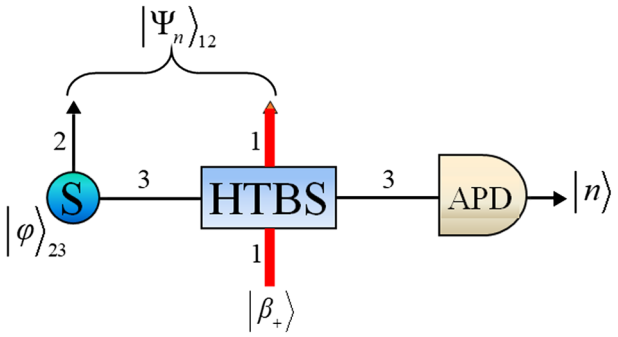

Fig. 1 A schematic representation for generation of the hybrid state $|\Psi_n\rangle_{12}$ in Eq. (9), using a highly transmissive beam splitter (HTBS) to mix a CV cat state $|\beta_+\rangle$ in Eq. (6a) with mode 3 of a DV state $|\varphi\rangle_{23}$ in Eq. (7), which is produced by a source S. APD is commercially achievable avalanche photodiode

on a Fox state $|n\rangle$ yields the so-called displaced number state $|n,\alpha\rangle$. The decomposition of $|n,\alpha\rangle$ in terms of Fox states as well as other relevant formulas are given in "Appendix A". Note that in (3), when $|\beta\rangle$ is replaced by $|-\beta\rangle$ one has

$$BS(\rho\otimes|-\beta\rangle\langle-\beta|)BS^{+}\approx D(-\alpha)\rho D^{+}(-\alpha)\otimes|-\beta\rangle\langle-\beta|. \tag{5}$$

Note that although β may be very large ($\beta\to\infty$) and r may be very small ($r\to 0$), one may control them so as to keep α in (4) finite, $\alpha=$ const. In real experiments, $r\neq 0$ and $\beta\neq\infty$, so the approximate sign is used in Eqs. (3) and (5).

Of interest in the CV framework are Schrödinger cat states which are superpositions of coherent states like these

$$|\beta\rangle_{+}=N_{+}(|-\beta\rangle+|\beta\rangle), \tag{6a}$$

$$|\beta_{-}\rangle=N_{-}(|-\beta\rangle-|\beta\rangle), \tag{6b}$$

where the factors $N_{\pm}=\left(2\left(1\pm\exp\left(-2\beta^{2}\right)\right)\right)^{-1/2}$ are the normalization parameters. As for the DV framework, the dual-rail state of a single photon involving two spatial modes of the form

$$|\varphi\rangle_{23}=a_0|01\rangle_{23}+a_1|10\rangle_{23}, \tag{7}$$

with $|a_0|^2+|a_1|^2=1$, plays an important role. The state (7) can be created by sending a photon through one input of a BS. If states (6a) and (7) are the two inputs of the HTBS (see Fig. 1), then, using the mathematical derivation detailed in "Appendix B", we have

$$BS_{13}\left(|\beta_{+}\rangle_1|\varphi\rangle_{23}\right)\to N_{+}F\sum_{n=0}^{\infty}\frac{c_{1n}(\alpha)}{N_nN_n^{(\mathrm{tot})}}|\Psi_n\rangle_{12}|n\rangle_3. \tag{8}$$

Here, we introduce the following two-mode entangled hybrid states

$$|\Psi_n\rangle_{12} = N_n^{(\mathrm{tot})}\Big(|-\beta\rangle_1\Big|\varphi_n^{(+)}\Big\rangle_2 + (-1)^{n-1}|\beta\rangle_1\Big|\varphi_n^{(-)}\Big\rangle_2\Big) \tag{9}$$

and the single-rail state of a photon composed of the vacuum and the single-photon states

$$\Big|\varphi_n^{(\pm)}\Big\rangle_2 = N_n(a_0|0\rangle_2 \pm a_1 A_n|1\rangle_2). \tag{10}$$

In the above expressions

$$N_n = \Big(|a_0|^2 + |a_1|^2|A_n|^2\Big)^{-1/2} = \Big(1 + \Big(|A_n|^2 - 1\Big)|a_1|^2\Big)^{-1/2}, \tag{11}$$

$$N_n^{(\mathrm{tot})} = \Big(2\Big(1 + (-1)^{n-1}N_n^2\exp\Big(-2\beta^2\Big)\Big(1 - \Big(1 + |A_n|^2\Big)|a_1|^2\Big)\Big)\Big)^{-1/2} \tag{12}$$

are the normalization factors, $F = \exp\big(-\alpha^2/2\big)$, while $c_{1n}(\alpha)$ and A_n are defined by (A15) and (B4). Clearly from (8), registration of n photons in mode 3 generates the state $|\Psi_n\rangle_{12}$ in Eq. (9), with a probability equal to

$$P_n(\alpha) = N_+^2 F^2 \frac{|c_{1n}(\alpha)|^2}{N_n^2 N_n^{(\mathrm{tot})2}}. \tag{13}$$

As it should be, the success probabilities sum up to 1, i.e., $\sum_{n=0}^{\infty} P_n(\alpha) = 1$, in the limit of $t \to 1$ ($r \to 0$), due to (A10).

2.2 Hybrid entanglement between a CV and a dual-rail DV states

Next, consider another type of DV–CV interaction with the DV state in the form of two-photon entanglement occupying simultaneously four spatial modes

$$|\phi\rangle_{3456} = a_0|0101\rangle_{3456} + a_1|1010\rangle_{3456}, \tag{14}$$

which can be created by sending each mode of the polarization-entangled state of the form $a_0|HV\rangle_{34} + a_1|VH\rangle_{34}$, with $H(V)$ denoting horizontal (vertical) polarization, through a polarization beam splitter. The optical scheme for this type of DV–CV interaction is shown in Fig. 2 which consists of two HTBSs. One HTBS mixes an even Schrödinger cat state $|\beta_+\rangle_1$, in Eq. (6a), with mode 5 of $|\phi\rangle_{3456}$, whereas an additional coherent state $|-\beta_1\rangle_2$ ($\beta_1 > 0$) is mixed on the other HTBS with mode 6 of $|\phi\rangle_{3456}$. Using the mathematical derivation detailed in "Appendix C" gives

$$\begin{aligned} &BS_{15}BS_{26}\big(|\beta_+\rangle_1|-\beta_1\rangle_2|\phi\rangle_{3456}\big) \\ &\quad\to N_+F^2|-\beta\rangle_2\sum_{n=0}^{\infty}\sum_{m=0}^{\infty}\frac{c_{0n}(\alpha)c_{1m}(\alpha_1)}{N_{nm}N_{nm}^{(\mathrm{tot})}}|\Psi_{nm}\rangle_{134}|nm\rangle_{56}, \end{aligned} \tag{15}$$

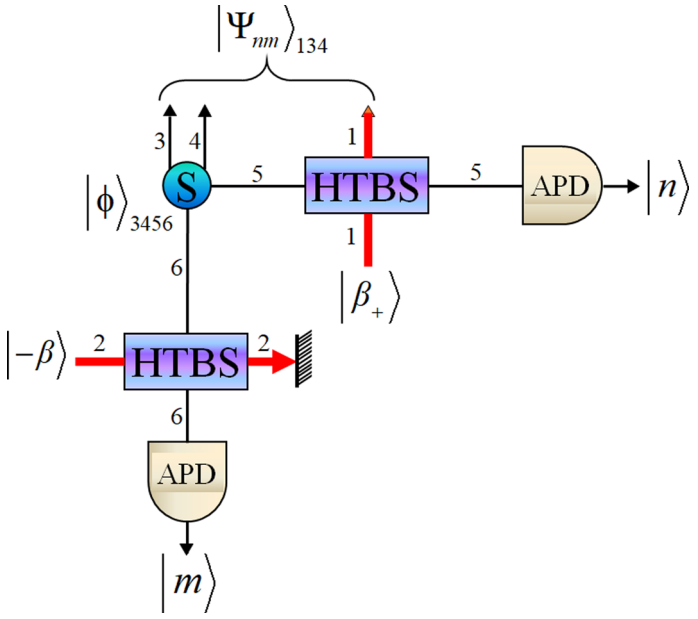

Fig. 2 A schematic representation for generation of the hybrid state $|\Psi_{nm}\rangle_{134}$ in Eq. (16), using two highly transmissive beam splitters (HTBSs), one (the other) is to mix a CV cat state $|\beta_+\rangle$ (coherent state $|-\beta\rangle$) with mode 5 (mode 6) of a DV state $|\varphi\rangle_{3456}$ in Eq. (14), which is produced by a source S. APD is commercially achievable avalanche photodiode

with finite $\alpha = \beta r$ and $\alpha_1 = \beta_1 r$,

$$|\Psi_{nm}\rangle_{134} = N_{nm}^{(\mathrm{tot})}\Big(|-\beta\rangle_1\Big|\varphi_{nm}^{(+)}\Big\rangle_{34} + (-1)^n|\beta\rangle_1\Big|\varphi_{nm}^{(-)}\Big\rangle_{34}\Big), \tag{16}$$

$$\Big|\varphi_{nm}^{(\pm)}\Big\rangle_{34} = N_{nm}(a_0|01\rangle_{34} \pm a_1 A_{nm}|10\rangle_{34}) \tag{17}$$

and the normalization factors

$$N_{nm} = \Big(|a_0|^2 + |a_1|^2|A_{nm}|^2\Big)^{-1/2} = \Big(1 + \Big(|A_{nm}|^2 - 1\Big)|a_1|^2\Big)^{-1/2}, \tag{18}$$

$$N_{nm}^{(\mathrm{tot})} = \Big(2\Big(1 + (-1)^n N_{nm}^2 \exp\Big(-2|\beta|^2\Big)\Big)\Big(1 - \Big(1 + |A_{nm}|^2\Big)|a_1|^2\Big)\Big)\Big)^{-1/2}, \tag{19}$$

with A_{nm} derived in (C11). From (15), it follows that co-detection of n photons in mode 5 and m photons in mode 6 leads to generation of the hybrid entangled state (16) that comprises CV coherent states with opposite-in-sign amplitudes and DV dual-rail single-photon states, with a probability in the large-t (small-r) limit equal to

$$P_{nm}(\alpha, \alpha_1) = N_+^2 F^2(\alpha) F^2(\alpha_1) \frac{|c_{0n}(\alpha)|^2 |c_{1m}(\alpha_1)|^2}{N_{nm}^2 N_{nm}^{(\mathrm{tot})2}}. \tag{20}$$

These success probabilities are already normalized for any α and α_1 since it is straightforward to verify from (A10) that $\sum_{n,m=0}^{\infty} P_{nm}(\alpha, \alpha_1) = 1$.

Let us now discuss physical basis of our generation schemes. The hybrid entangled states in Eqs. (9) and (16) are generated if all the amplitude information of the CV state is erased. To erase this information, measurements aim to detect photon numbers in the auxiliary modes. The key point in our problem is then the decomposition of displaced number states over Fock ones (A6). The matrix elements $c_{ln}(\alpha)$ are written in (A8) as α^{n-l} times a bracketed factor. Since the bracketed factor depends only on the absolute value of the displacement amplitude $|\alpha|$, it is invariant with respect to the transformation $\alpha \to \alpha \exp(i\varphi)$ with any angle φ. As for α^{n-l}, it determines the phase of the matrix elements when the displacement amplitude is rotated in the phase plane. So, the matrix elements $c_{0n}(\alpha)$ are those of the coherent state as seen in (A14) and acquire a factor $(-1)^n$ under the change $\alpha \to -\alpha$. As for the matrix elements $c_{1n}(\alpha)$ in Eq. (A15), it determines the displaced single photon and acquires a factor $(-1)^{n-1}$ under the same change $\alpha \to -\alpha$. This difference in the way the matrix elements $c_{ln}(\alpha)$ change in accordance with the change in the parity of the displaced state is akin to the nonlinear action of two-qubit controlled-Z gate. Note, however, that this mechanism does not work for the target entangled states in the polarization encoding like

$$|\varphi\rangle_2 = a_0|H\rangle_{23} + a_1|V\rangle_2, \tag{21}$$

or

$$|\phi\rangle_{34} = a_0|HV\rangle_{34} + a_1|VH\rangle_{34}, \tag{22}$$

as the states $|H\rangle$ and $|V\rangle$, though have different polarizations, possess the same parity. The coherent components of the cat (6a) simultaneously displace the target qubit in indistinguishable manner on HTBS by the values which have opposite signs. All information about the displaced values experienced by the target qubit disappears after the measurement, and this uncertainty forms the superposed hybrid state. Additional amplitude factors A_n in (10) and A_{nm} in (17) appear as inherent parts of the DV–CV interaction on HTBS. A coherent auxiliary state $|-\beta\rangle_2$ in mode 2 is used to realize the state (16). This state does not change the sign of $c_{0n}(\alpha)$ and $c_{1n}(\alpha)$.

To assess the quality of our schemes, we calculate the fidelities Fid_n and Fid_{nm} between the states (9) and (16), which are obtained in the large-t (small-r) limit, and the actual ones, which are generated with finite t and r. Using the expression (B16) in "Appendix B," we have

$$\mathrm{Fid}_n = \left(N_n^{(\mathrm{tot})}(\beta) N_n^{(\mathrm{tot})}(\beta/t) N_n^{(\mathrm{tot})'}(\beta)\right)^2, \tag{23}$$

with $N_n^{(\mathrm{tot})}(\beta)$ and $N_n^{(\mathrm{tot})}(\beta/t)$ given by Eq. (12), while

$$N_n^{(\mathrm{tot})'}(\beta) = 2\begin{pmatrix} \exp\left(-\frac{|\beta|^2}{2}\left(1-\frac{1}{t}\right)^2\right) + (-1)^{n-1} N_n^2 \exp\left(-\frac{|\beta|^2}{2}\left(1+\frac{1}{t}\right)^2\right) \\ \left(1-\left(1+|A_n|^2\right)|a_1|^2\right) \end{pmatrix} \tag{24}$$

and

$$\mathrm{Fid}_{nm} = \left(N_{nm}^{(\mathrm{tot})}(\beta) N_{nm}^{(\mathrm{tot})}(\beta/t) N_{nm}^{(\mathrm{tot})'}(\beta)\right)^2, \tag{25}$$

with $N_{nm}^{(\mathrm{tot})}(\beta)$ and $N_{nm}^{(\mathrm{tot})}(\beta/t)$ given by Eq. (19), while $N_{nm}^{(\mathrm{tot})'}(\beta)$ follows from Eq. (24) by the substitutions $A_n \to A_{nm}$ and $N_n \to N_{nm}$. In the general case, the fidelities depend in a complex manner on the parameters of the experimental setup, the amplitude of the coherent components, the displacement amplitude α and the value of the absolute value $|a_1|$ of the target states in (7) and (14).

3 Balanced hybrid entangled states

The states (9) and (16) in the previous section are hybrid entangled, but unbalanced in the sense that their component terms are in general not equally weighted, i.e., $|a_0| \neq |a_1||A_n|$ in (10) and $|a_0| \neq |a_1||A_{nm}|$ in (17), respectively. Interestingly, we can establish the conditions to obtain balanced hybrid entangled states by adjusting the initial parameters. Namely, the condition is $|a_0|^2 = |A_n|^2/\left(1+|A_n|^2\right)$ and $|a_1|^2 = 1/\left(1+|A_n|^2\right)$, under which after registering n photons in mode 3 of Fig. 1, the state (9) becomes

$$\left|\Psi_n^{(b)}\right\rangle_{12} = \frac{1}{2}\Big(|-\beta\rangle_1(|0\rangle_2 + |1\rangle_2) + (-1)^{n-1}|\beta\rangle_1(|0\rangle_2 - |1\rangle_2)\Big), \tag{26}$$

where the superscript (b) means "balanced" and the zero relative phase between a_0 and a_1 is assumed. Applying on mode 2, the Hadamard transformation $H = |0\rangle(\langle 0| + \langle 1|)/\sqrt{2} + |1\rangle(\langle 0| - \langle 1|)/\sqrt{2}$ brings (26) to

$$\left|\Psi_n^{(b)}\right\rangle_{12} = \frac{1}{\sqrt{2}}\Big(|-\beta\rangle_1|0\rangle_2 + (-1)^{n-1}|\beta\rangle_1|1\rangle_2\Big), \tag{27}$$

which is both balanced and hybrid. The corresponding success probability and fidelity are

$$P_n^{(b)}(\alpha) = 4N_+^2F^2|c_{1n}(\alpha)|^2\frac{|A_n(\alpha)|^2}{1+|A_n(\alpha)|^2}, \tag{28}$$

and

$$\mathrm{Fid}_n^{(b)} = \exp\left(-|\alpha|^2\frac{1-t}{1+t}\right). \tag{29}$$

We plot in Fig. 3 the dependence of $P_0^{(b)}$, $P_1^{(b)}$, $P_n^{(b)}(t=0.9)$ and $\mathrm{Fid}_0^{(b)} = \mathrm{Fid}_1^{(b)}$, respectively, on the displacement amplitude α for different values of the transmittance t. These top-left and top-right subfigures reveal that both the probabilities $P_0^{(b)}$ and $P_1^{(b)}$ increase with increasing t for small values of α, but turn out insensitive to t when

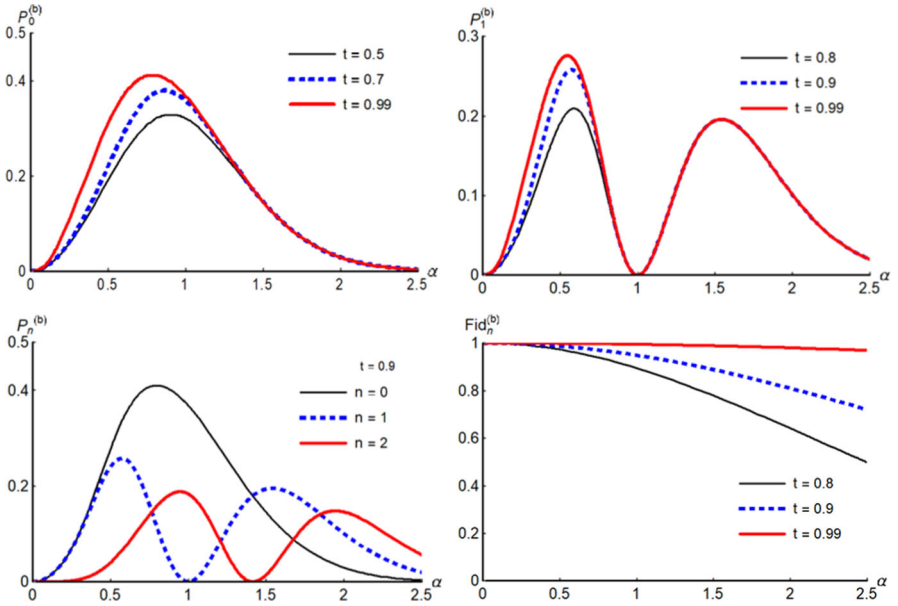

Fig. 3 Success probability, Eq. (28), $P_0^{(b)}$ (top-left), $P_1^{(b)}$ (top-right), $P_{0,1,2}^{(b)}$ (bottom-left) and fidelity, Eq. (29), $Fid_n^{(b)}$ (bottom-right) as functions of α for different values of t and n as indicated in each subfigure

α becomes large. For a given t, the success probability $P_n^{(b)}$ depends on both α and n (as in the bottom-left subfigure of Fig. 3 for $t = 0.9$), showing on average a favor to a smaller value of n. However, as seen from the bottom-right subfigure of Fig. 3, the fidelity $\mathrm{Fid}_n^{(b)}$ is independent of n and becoming better when t is getting closer to 1, for the whole range of α. From the values of the displacement amplitude, we can get the value β of the even cat size, using the relation (4).

Likewise, the generally unbalanced hybrid entangled state (16) can also be made balanced by suitably tailoring the problem's parameters under detection of certain photon numbers in mode 5 and mode 6 in Fig. 2. Namely, if we impose the condition $a_0 = a_1 A_{nm}$, then from (17)–(19) we have $N_{nm} = 1/\left(|a_0|\sqrt{2}\right)$, $N_{nm}^{(\mathrm{tot})} = 1/\sqrt{2}$, $\left|\varphi_{nm}^{(\pm)}\right\rangle = (|01\rangle_{23} \pm |10\rangle_{23})/\sqrt{2}$ and therefore, the unbalanced state becomes

$$\left|\Psi_{nm}^{(b)}\right\rangle_{123} = \frac{1}{2}\left(|-\beta\rangle_1(|01\rangle_{23} + |10\rangle_{23}) + (-1)^n|\beta\rangle_1(|01\rangle_{23} - |10\rangle_{23})\right), \tag{30}$$

which can be transformed into

$$\left|\Psi_{nm}^{(b)}\right\rangle_{123} = \frac{1}{\sqrt{2}}\left(|-\beta\rangle_1|01\rangle_{23} + (-1)^n|\beta\rangle_1|10\rangle_{23}\right), \tag{31}$$

by applying the Hadamard transformation to the dual-rail single-photon state of modes 2 and 3 [30]. It is worthy to note that the balanced state (31) is obtained not for

any registered photon numbers n and m, but only for those satisfying the condition $a_0 = a_1 A_{nm}$ we imposed above. More explicitly, by virtue of Eq. (C11), for given parameters $\{a_0, a_1, \alpha, \alpha_1\}$, n and m should be related so that $a_0\alpha\left(m - |\alpha_1|^2\right) = a_1\alpha_1\left(n - |\alpha|^2\right)$. In particular, if we set $a_0 = a_1 = 1/\sqrt{2}$ and $\alpha = \alpha_1$, then a balanced hybrid entanglement is generated whenever $n = m$. The corresponding success probability can then be derived as

$$P_{nn}^{(b)}(\alpha) = 2N_+^2 F^4(\alpha)|c_{0n}(\alpha)|^2|c_{1n}(\alpha)|^2. \tag{32}$$

The fidelity to generate the state (30) coincides with (29) derived for production of the state (26). If the numbers of photons detected in modes 5 and 6 in Fig. 2 are different, i.e., $n \neq m$, then some terms of the superposition state

$$|\Psi_{nm}\rangle_{123} = N_{nm}^{(\mathrm{tot})}\left(|-\beta\rangle_1 N_{nm}(|01\rangle_{23} + A_{nm}|10\rangle_{23})/\sqrt{2} + (-1)^n|\beta\rangle_1 N_{nm}(|01\rangle_{23} - A_{nm}|10\rangle_{23})/\sqrt{2}\right) \tag{33}$$

acquire an additional amplitude factor A_{nm} in the case of $|a_0| = |a_1| = 1/\sqrt{2}$. The dependencies of $P_{00}^{(b)}(\alpha)$ and $P_{11}^{(b)}(\alpha)$ on the displacement amplitude α are shown in the top-left and top-right subfigure of Fig. 4, respectively, for different values of the experimental parameter t. As can be seen from the subfigures, an increase in t leads to a slight increase in the success probabilities under small values of α. In case of $n \neq m$ (see the bottom-left subfigure of Fig. 4) shows the dependence of $P_{01}(\alpha) = P_{10}(\alpha)$ on α : the probabilities decrease with increasing α. Note that the state (31) can also be transformed into the hybrid entangled state with single photon in polarization basis

$$\left|\Psi_{nn}^{(b)}\right\rangle_{12} = \frac{1}{\sqrt{2}}\left(|-\beta\rangle_1|H\rangle_2 + (-1)^n|\beta\rangle_1|V\rangle_2\right) \tag{34}$$

with the help of a polarizer and a polarization beam splitter. In practice, implementing the Hadamard operation for a single-rail qubit by linear optics is a rather complicated problem. But, we can realize the state (27) by the same technique that was used to generate the states (9) and (16). Mixing mode 3 of the state (31) with a coherent state with some amplitude β_2 chosen such that $c_{0n}(\gamma) = c_{1n}(\gamma)$, where β_2 and γ are connected by the relation (4), and registering n photons in the auxiliary mode, the state to be obtained is that of (27). This condition is satisfied in the case of the displacement amplitude $\gamma_1 = \left(-1 + \sqrt{1+4n}\right)/2$ and $\gamma_2 = \left(-1 - \sqrt{1+4n}\right)/2$.

At this moment, we would like to remark that the balanced state (30) but not state (33) will also be obtained under another condition $a_0 = -a_1 A_{nm}$, which for $a_0 = a_1 = 1/\sqrt{2}$ implies $A_{nm} = -1$. Then, for $\alpha = \alpha_1$, the detected photon numbers n and m that herald the generation of state (30) obey the relation $n + m = 2|\alpha|^2$. This clearly reveals that n and m could be largely different if $|\alpha|^2 \gg 1$. In particular, when either $n = 0$, $m = 1$ or $n = 1$, $m = 0$ we have $|\alpha| = 1/\sqrt{2}$. With this value of the displacement amplitude, it turns out that the state (30) is indeed generated for the measurement outcomes being either $|01\rangle_{56}$ or $|10\rangle_{56}$. The bottom-right subfigure of Fig. 4 shows the dependence of the success probability to realize the state (30) on the transmittance t in the case of $|\alpha| = 1/\sqrt{2}$. Here, four measurement outcomes $|00\rangle_{56}$,

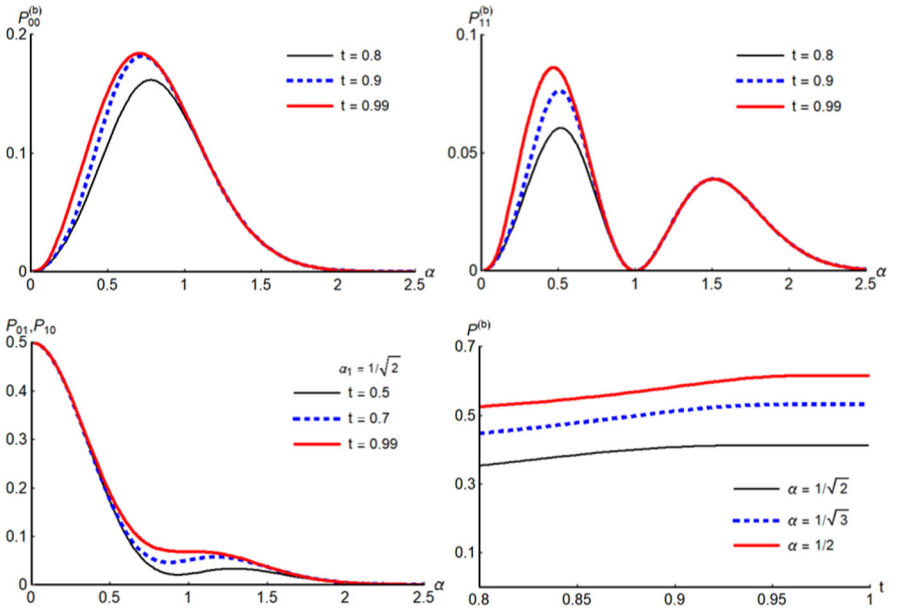

Fig. 4 Success probabilities, Eq. (32), $P_{00}^{(b)}$ (top-left), $P_{11}^{(b)}$ (top-right), the success probability, Eq. (20), $P_{01} = P_{10}$ (bottom-left) and the sum of some success probabilities $P^{(b)} = P_{00}^{(b)} + P_{11}^{(b)} + P_{01} + P_{10}$ (bottom-right) of producing the hybrid entangled states (30) and (33) with $|a_0| = |a_1| = 1/\sqrt{2}$ in (14) as functions of α or t for different parameters indicated in the figure legends. The black curve in the bottom-right subfigure corresponds exclusively to the generation of the balanced state (30)

$|01\rangle_{56}$, $|10\rangle_{56}$ and $|11\rangle_{56}$ give their contribution to the generation. The probability of success is increased in this situation compared to that in the top-left and top-right subfigure of Fig. 4.

More generally, relaxing any constraints on α, α_1 the state (30) appears for arbitrary $n \neq m$ if the condition $|a_0| = |a_1||A_{nm}|$ is imposed, which is valid when $|a_1|^2 = 1/\left(1 + |A_{nm}|^2\right)$. Then, if n and m photons are registered in mode 5 and mode 6, respectively, the state (30) is generated with the probability

$$P_{nm}^{(b)}(\alpha) = 4N_+^2 F^4 |c_{0n}(\alpha)|^2 |c_{1n}(\alpha)|^2 \frac{|A_{nm}(\alpha, \alpha_1)|^2}{1 + |A_{nm}(\alpha, \alpha_1)|^2} \tag{35}$$

and the fidelity given by Eq. (29). Note that expression (35) goes into formula (32) in the case of $n = m$ as $|A_{nn}(\alpha, \alpha_1)| = 1$ for $\alpha = \alpha_1$. Numerical results show similar dependencies of the success probability on the displacement amplitude as in Fig. 4.

The possibility to generate the hybrid state with coherent and one-photon single-rail components was experimentally demonstrated [19] with the target being the two-mode squeezed state

$$|\varphi_1\rangle_{si} = N_\lambda(|00\rangle_{si} + \lambda|11\rangle_{si}), \tag{36}$$

which appears as output from optical parametric down-conversion for the signal s and idler i modes in the very low gain limit, with N_λ the normalization factor. Then, using the same calculation technique for Fig. 1a, we can obtain the state (9) with one-photon single-rail components

$$\left|\varphi_n^{(\pm)}\right\rangle_2 = N_n\left(|0\rangle_2 \pm \lambda A_n^{-1}|1\rangle_2\right). \tag{37}$$

The success probability in this setup is the same as given by Eq. (13) with c_{1n} (α) and A_{nm} replaced by $c_{0n}(\alpha)$ and A_{nm}^{-1}, respectively. By imposing the condition $\lambda A_n^{-1} = 1$, the balanced hybrid entangled state (26) can be produced.

Finally, we also give an example of hybrid converter enabling to map discrete qubits to coherent state ones. Let us take the state (31) and use a beam splitter to perform the transformations $|01\rangle_{23} \to t|01\rangle_{23} + r|10\rangle_{23}$ and $|10\rangle_{12} \to t|10\rangle_{12} - r|01\rangle_{12}$. Then, due to simultaneous presence of a single photon in both modes and indistinguishability between the events, the following superpositions of coherent states

$$|\Phi_1\rangle_1 = N_1(t|-\beta\rangle - r|\beta\rangle)_1 \tag{38a}$$

and

$$|\Phi_2\rangle_1 = N_2(r|-\beta\rangle + r|\beta\rangle)_1, \tag{38b}$$

with $N_{1,2}$ the corresponding normalization factors, are expected to obtain, provided that the following measurement outcomes $|01\rangle_{23}$ and $|10\rangle_{23}$, respectively, are found. The states (38a) and (38b) can be considered as CV qubits subjected to a one-qubit transformation in basis $|\pm\beta\rangle$.

4 Degree of entanglement

The hybrid entangled states (27) and (31) are though balanced, but this does not mean that they are maximally entangled. The reason rests in the non-orthogonality of the component coherent states which have the same size but opposite signs. To evaluate to which extent those states are entangled (i.e., the degree of their entanglement), a relevant entanglement measure should be used and computed. One of the entanglement measures is the so-called negativity [31] which is easy to compute in a four-dimensional Hilbert space. This quantity is derived from the positive partial transpose (PPT) criterion for separability [32] and possesses all required properties for the entanglement measure. The negativity $\mathcal{N}$ of a bipartite composed system AB characterized by a density matrix ϱ is defined by $\mathcal{N} = \left(\left\|\varrho^{T_A}\right\| - 1\right)/2$, where ϱ^{T_A} is the partial transpose of ϱ with respect to the subsystem A and $\left\|\varrho^{T_A}\right\| = Tr\left|\varrho^{T_A}\right| = Tr\sqrt{\left(\varrho^{T_A}\right)^+\varrho^{T_A}}$ is the trace norm of the sum of the singular values of the operator ϱ^{T_A}, where $\left(\varrho^{T_A}\right)^+$ means Hermitian conjugate operator of original ϱ^{T_A}. The maximum value of the negativity of a quantum state is one, i.e., $\mathcal{N}_{max} = 1$, which

indicates that the corresponding state is maximally entangled. For the states (27) and (31), our calculation yields

$$\mathcal{N} = \sqrt{1 - \exp\left(-4|\beta|^2\right)}, \tag{39}$$

which tends to 1 ($\mathcal{N} \to \mathcal{N}_{\max}$) in the case of an infinitely large value of the amplitude of the coherent states, i.e., $|\beta| \to \infty$. Thus, mathematically, the balanced hybrid states (27) and (31) are non-maximally entangled for a finite $|\beta|$. However, since exp $\left(-4|\beta|^2\right)$ drops very quickly with increasing $|\beta|$, these states can be considered as (near-)maximally entangled for sufficiently large values of the amplitude $|\beta|$ as in our cases.

Alternatively, we can also assess the degree of entanglement by another convenient measure called concurrence C [33]. For the most general pure state of a two-qubit system $|\Omega\rangle_{12} = a|\bar{0}\rangle_1|\bar{0}\rangle_2 + b|\bar{0}\rangle_1|\bar{1}\rangle_2 + c|\bar{1}\rangle_1|\bar{0}\rangle_2 + d|\bar{1}\rangle_1|\bar{1}\rangle_2$ with $\{|\bar{0}\rangle_1, |\bar{1}\rangle_1\}, \{|\bar{0}\rangle_2, |\bar{1}\rangle_2\}$ some orthonormal basis for qubit 1 (2) and $|a|^2 + |b|^2 + |c|^2 + |d|^2 = 1$, the concurrence is determined by

$$\mathrm{C} = 2|ad - bc|. \tag{40}$$

Now, to calculate the concurrence of the state (27), we make use of the Gram–Schmidt theorem to build an orthonormal basis for the coherent states as $|\bar{0}\rangle = |\beta\rangle$ and $|\bar{1}\rangle = (|-\beta\rangle - Z|\beta\rangle)/\sqrt{1 - Z^2}$, with $Z = \langle\beta|-\beta\rangle = \exp\left(-2|\beta|^2\right)$ [34]. Then, the state (27), in terms of $\{|\bar{0}\rangle_1, |\bar{1}\rangle_1\}$ and $\{|\bar{0}\rangle_2 \equiv |0\rangle_2, |\bar{1}\rangle_2 \equiv |1\rangle_2\}$, becomes

$$\left|\Psi_n^{(b)}\right\rangle_{12} = \frac{1}{\sqrt{2}}\left(Z|\bar{0}\rangle_1|\bar{0}\rangle_2 + (-1)^{n-1}|\bar{0}\rangle_1|\bar{1}\rangle_2 + \sqrt{1 - Z^2}|\bar{1}\rangle_1|\bar{0}\rangle_2\right). \tag{41}$$

Similarly, for the state (31), in terms of $\{|\bar{0}\rangle_1, |\bar{1}\rangle_1\}$ and $\{|\bar{0}\rangle_2 \equiv |01\rangle_{23}, |\bar{1}\rangle_2 \equiv |10\rangle_{23}\}$, we have

$$\left|\Psi_{nm}^{(b)}\right\rangle_{12} = \frac{1}{\sqrt{2}}\left(Z|\bar{0}\rangle_1|\bar{0}\rangle_2 + (-1)^{n}|\bar{0}\rangle_1|\bar{1}\rangle_2 + \sqrt{1 - Z^2}|\bar{1}\rangle_1|\bar{0}\rangle_2\right). \tag{42}$$

From (41) and (42), it immediately follows by virtue of (40) that the concurrence of both the states (27) and (31) is $C = \sqrt{1 - Z^2}$ which exactly coincides with the negativity $\mathcal{N}$ derived in (39) above.

5 Conclusion

We have developed the theory of interactions between the discrete-variable and continuous-variable (DV–CV interaction) states on highly transmissive beam splitters (HTBSs). Generation of the hybrid entanglement between DV states (single photons) and CV ones (coherent states) has special interest in fundamental quantum mechanics within the framework of demonstration of Schrödinger cat states [13]. The theory is based on peculiarities of the DV–CV interaction by means of HTBS. Manipulations

with DV and CV states are pretty well known, while the DV–CV interaction is a fairly new and less known problem, so designing such interactions would bring notable advantages for the implementation of quantum protocols [17]. Coherent components of a Schrödinger cat state with opposite-in-sign amplitudes simultaneously displace the target microscopic state in an indistinguishable manner if the subsequent registration of photons in the auxiliary mode is made. This indistinguishability gives rise to generation of a set of the hybrid entangled states whose amplitudes differ from each other by known values. The change in sign of the displacement amplitude leads to the fact that the amplitudes of the decomposition of the displaced states of light vary depending on the overall parity of the photon being registered and the target displaced state. Thus, the hybrid entanglement arises irrespective of the number of registered photons due to action of the mechanism of DV–CV interactions. In general, the generated hybrid states are unbalanced (i.e., their component terms are unequally weighted), but the initial parameters of the generation scheme can be chosen so as to equalize the weights of the hybrid states making them balanced.

Here, two optical schemes to realize two different types of hybrid entangled states have been proposed. One of them (see Eq. (9)) is formed from coherent components and single-rail qubit composed of the vacuum and the one-photon states. Either state of a single photon occupying two modes as in Eq. (7) or two-mode squeezed state with small value of the squeezing parameter as in Eq. (36) can be served as the target state for generation of the hybrid states. The other type of hybrid entanglement of the form of Eq. (16) can be obtained by using two-photon four-mode state as in Eq. (14) as the target one. Moreover, by generating the hybrid states (31) with dual-rail photon as components, one can also transform them to those in polarization basis as in Eq. (34). The proposed schemes can generate balanced hybrid states with near-maximal entanglement under certain conditions which have been established in this work. The success probabilities to generate the states of concern in dependence on the displacement amplitude, and the HTBS parameter are obtained analytically and shown graphically. The best strategies to generate the balanced hybrid states with the greatest success probabilities and maximum fidelities are considered as well. The schemes rely on a probabilistic preparation heralded by detecting the photon numbers. In this way, noisy environment only affects the count rate but not the fidelity of the resulting states. Therefore, the proposed method is more suitable to create entanglement between different subsystems that differ in size or in the way they are most conveniently described in DV and CV framework. Note that the implementation of the optical circuits presented here requires a minimum irreducible number of optical elements, thus increasing the effectiveness of our schemes.

Finally, we would like to note that superpositions of coherent states (SCSs) in the form of Eqs. (6a) and (6b) are not the only ones that can be exploited to generate the concerned hybrid entanglement. As a matter of practical experience, instead of the states (6a) and (6b), researchers use other CV states that approximate them quite well [35, 36]. Yet, then the following question may be raised: how good is the DV–CV interaction for the generation of hybrid entanglement if the SCSs are replaced by their analogues with good fidelity? Even though superposition of coherent states may be substituted by squeezed vacuum for small size, while squeezed single photon may approximate odd superposition of coherent states of larger amplitude, consideration

of such delicate issues are beyond the scope of the present work but deserves separate analysis. Nevertheless, it can be expected that the designed DV–CV interaction mechanisms may also generate hybrid entanglement with high fidelity by using CV states other than ECSs, implying the universality of our designs.

Acknowledgements S.A.P. is supported by Act 211 Government of the Russian Federation, contract No. 02.A03.21.0011, while N.B.A. is supported by the National Foundation for Science and Technology Development (NAFOSTED) under Project No. 103.01-2017.08.

Appendix A: Decomposition of displaced number state in terms of Fock states

The displacement operator $D(\alpha)$ is unitary and determined by

$$D(\alpha) = \exp\left(\alpha a^{+} - \alpha^{*} a\right), \tag{A1}$$

with α the displacement amplitude and $a(a^{+})$ the bosonic annihilation (creation) operator. Its action on an arbitrary pure state

$$|\psi\rangle = \sum_{n=0}^{k} a_n |n\rangle, \text{ with } \sum_{n=0}^{k} |a_n|^2 = 1, \tag{A2}$$

reads

$$D(\alpha)|\psi\rangle = \sum_{n=0}^{k} a_n |n, \alpha\rangle, \tag{A3}$$

where

$$|n, \alpha\rangle = D(\alpha)|n\rangle \tag{A4}$$

is called a displaced number state, which is characterized by two numbers: a quantum discrete number n and a classical continuous parameter α (α specifies the size of the state [23]). Note that $|0, \alpha\rangle = D(\alpha)|0\rangle = |\alpha\rangle$ is nothing else but the coherent state. For a given α the states

$$\{|n, \alpha\rangle, n = 0, 1, 2, \ldots, \infty\}, \tag{A5}$$

with the inner products $\langle n, \alpha | m, \alpha\rangle = \delta_{nm}$ constitute the basic set of the displaced number state. The decomposition of a displaced number state in terms of Fock states is [23]

$$|l, \alpha\rangle = F \sum_{n=0}^{\infty} c_{ln}(\alpha)|n\rangle, \tag{A6}$$

with $F = \exp\left(-|\alpha|^2/2\right)$ and $c_{ln}(\alpha)$ are determined in [26] by

$$c_{ln}(\alpha) = \frac{\alpha^{n-l}}{\sqrt{l!\,n!}} \sum_{k=0}^{l} (-1)^k C_l^k |\alpha|^{2k} \prod_{k=0}^{l-1} (n-l+k+1), \tag{A7}$$

or the same

$$c_{ln}(\alpha) = \frac{\alpha^{n-l}}{\sqrt{l!\,n!}} \left(\begin{array}{r} n(n-1)\ldots(n-l+1) - C_l^1 |\alpha|^2 n(n-1)\ldots(n-l+2) \\ +C_l^2 |\alpha|^4 n(n-1)\ldots(n-l+3) + \cdots \\ +(-1)^k C_l^k |\alpha|^{2k} \prod_{k}^{l-1} (n-l+k+1) + (-1)^l |\alpha|^{2l} \end{array} \right), \tag{A8}$$

where $C_l^k = l!\,/(k!\,(l-k)!)$ and

$$\prod_{k}^{l-1} (n-l+k+1) = n(n-1)\ldots(n-l+k+1). \tag{A9}$$

The matrix elements $c_{mn}(\alpha)$ in (A7) satisfy the normalization condition [26]

$$F^2 \sum_{n=0}^{\infty} |c_{ln}(\alpha)|^2 = 1. \tag{A10}$$

From the explicit expressions (A7) or (A8) of $c_{ln}(\alpha)$, it is possible to check the following relation

$$c_{ln}(-\alpha) = (-1)^{n-l} c_{ln}(\alpha). \tag{A11}$$

Obviously, for even l (i.e., $l = 2m$)

$$c_{2m,n}(-\alpha) = (-1)^n c_{2m,n}(\alpha), \tag{A12}$$

and for odd l (i.e., $l = 2m+1$)

$$c_{2m+1,n}(-\alpha) = (-1)^{n-1} c_{2m+1,n}. \tag{A13}$$

In particular, for $l = 0$ and $l = 1$ one has [26]

$$c_{0n}(\alpha) = \frac{\alpha^n}{\sqrt{n!}}, \tag{A14}$$

$$c_{1n}(\alpha) = \frac{\alpha^{n-1}}{\sqrt{n!}} \left(n - |\alpha|^2\right), \tag{A15}$$

satisfying the normalization conditions

$$F^2\sum_{n=0}^{\infty}|c_{0n}(\alpha)|^2=1, \tag{A16}$$

$$F^2\sum_{n=0}^{\infty}|c_{1n}(\alpha)|^2=1. \tag{A17}$$

One also has

$$c_{0n}(-\alpha)=(-1)^n c_{0n}(\alpha), \tag{A18}$$

$$c_{1n}(-\alpha)=(-1)^{n-1}c_{1n}(\alpha). \tag{A19}$$

Appendix B: DV–CV interaction for generation of hybrid entangled states (9)

The action of HTBS on an even cat (6a) and a dual-rail one-photon state (7),

$$BS_{13}\big(|\beta_+\rangle_1|\varphi\rangle_{23}\big)=N_+\big(BS_{13}\big(|-\beta\rangle_1|\varphi\rangle_{23}\big)+BS_{13}\big(|\beta\rangle_1|\varphi\rangle_{23}\big)\big), \tag{B1}$$

can be calculated term by term as follows. For the first term in the RHS of (B1), we have

$$\begin{aligned}BS_{13}\big(|-\beta\rangle_1|\varphi\rangle_{23}\big)&=BS_{13}D_1(-\beta)D_3(-\alpha)BS_{13}^{+}BS_{13}|0\rangle_1 D_3(\alpha)|\varphi\rangle_{23}\\&=D_1(-\beta/t)D_3(0)BS_{13}|0\rangle_1(a_0|0\rangle_2|1,\alpha\rangle_3+a_1|1\rangle_2|\alpha\rangle_3)\\&=FD_1(-\beta/t)\sum_{n=0}^{\infty}c_{1n}(\alpha)(a_0|0\rangle_2+a_1A_n|1\rangle_2)BS_{13}(|0n\rangle_{13}),\end{aligned} \tag{B2}$$

while the second term reads

$$\begin{aligned}BS_{13}\big(|\beta\rangle_1|\varphi\rangle_{23}\big)&=BS_{13}D_1(\beta)D_3(\alpha)BS_{13}^{+}BS_{13}|0\rangle_1 D_3(-\alpha)|\varphi\rangle_{23}\\&=D_1(\beta/t)D_3(0)BS_{13}|0\rangle_1(a_0|0\rangle_2|1,-\alpha\rangle_3+a_1|1\rangle_2|-\alpha\rangle_3)\\&=FD_1(-\beta/t)\sum_{n=0}^{\infty}(-1)^{n-1}c_{1n}(\alpha)(a_0|0\rangle_2-a_1A_n|1\rangle_2)BS_{13}(|0n\rangle_{13}).\end{aligned} \tag{B3}$$

In (B2) and (B3)

$$A_n(\alpha)=\frac{c_{0n}(\alpha)}{c_{1n}(\alpha)}=\frac{\alpha}{n-|\alpha|^2}. \tag{B4}$$

Summing up (B2) and (B3) yields

$$BS_{13}\left(|\beta_+\rangle_1|\varphi\rangle_{23}\right) = FN_+\left(\begin{array}{r}|\Delta_0(-\beta)\rangle_{123}+|\Delta_0(\beta)\rangle_{123}+r\left(|\Delta_1(-\beta)\rangle_{123}+|\Delta_1(\beta)\rangle_{123}\right)\\ +r^2\left(|\Delta_2(-\beta)\rangle_{123}+|\Delta_2(\beta)\rangle_{123}\right)+\cdots\end{array}\right), \tag{B5}$$

where

$$|\Delta_0(-\beta)\rangle_{123} = |-\beta/t\rangle_1\sum_{n=0}^{\infty}c_{1n}(\alpha)t^n(a_0|0\rangle_2+a_1A_n|1\rangle_2)|n\rangle_3, \tag{B6}$$

$$|\Delta_0(\beta)\rangle_{123} = |\beta/t\rangle_1\sum_{n=0}^{\infty}(-1)^{n-1}c_{1n}(\alpha)t^n(a_0|0\rangle_2-a_1A_n|1\rangle_2)|n\rangle_3, \tag{B7}$$

$$|\Delta_1(-\beta)\rangle_{123} = |1,-\beta/t\rangle_1\sum_{n=1}^{\infty}c_{1n}(\alpha)t^{n-1}\sqrt{n}(a_0|0\rangle_2+a_1A_n|1\rangle_2)|n-1\rangle_3, \tag{B8}$$

$$|\Delta_1(\beta)\rangle_{123} = |1,\beta/t\rangle_1\sum_{n=1}^{\infty}(-1)^{n-1}c_{1n}(\alpha)t^{n-1}\sqrt{n}(a_0|0\rangle_2-a_1A_n|1\rangle_2)|n-1\rangle_3, \tag{B9}$$

$$|\Delta_2(-\beta)\rangle_{123} = |2,-\beta/t\rangle_1\sum_{n=2}^{\infty}c_{1n}(\alpha)t^{n-2}\sqrt{\frac{n(n-1)}{2!}}(a_0|0\rangle_2+a_1A_n|1\rangle_2)|n-2\rangle_3, \tag{B10}$$

$$|\Delta_2(\beta)\rangle_{123} = |2,\beta/t\rangle_1\sum_{n=2}^{\infty}(-1)^{n-1}c_{1n}(\alpha)t^{n-2}\sqrt{\frac{n(n-1)}{2!}}(a_0|0\rangle_2-a_1A_n|1\rangle_2)|n-2\rangle_3. \tag{B11}$$

Using the above expressions, we can obtain the formulas (8)–(12) in Sect. 2.1.

The fidelity Fid_n in (23) is derived as follows. If n photons are registered in mode 3 of Fig. 1(a), then we have, up to the first order of smallness of r,

$$\left|\Psi_r^{(n)}\right\rangle_{12} = N_r^{(n)}\left(\left|\Psi_0^{(n)}\right\rangle_{12}+r\sqrt{n+1}\frac{c_{1n+1}}{c_{1n}}\left|\Psi_1^{(n)}\right\rangle_{12}\right), \tag{B12}$$

where

$$\left|\Psi_0^{(n)}\right\rangle_{12} = N_n^{(\mathrm{tot})}(\beta/t)\left(|-\beta/t\rangle_1\left|\varphi_n^{(+)}\right\rangle_2+(-1)^{n-1}|\beta/t\rangle_1\left|\varphi_n^{(-)}\right\rangle_2\right), \tag{B13}$$

$$\left|\Psi_1^{(n)}\right\rangle_{12} = N_{n1}^{(\mathrm{tot})}(\beta/t)\left(|1,-\beta/t\rangle_1\left|\varphi_{n+1}^{(+)}\right\rangle_2+(-1)^{n}|1,\beta/t\rangle_1\left|\varphi_{n+1}^{(-)}\right\rangle_2\right), \tag{B14}$$

with $N_n^{(\mathrm{tot})}$ (Eq. (12)) and $N_{n1}^{(\mathrm{tot})}$ the corresponding normalization factors. As for the normalization factor $N_r^{(n)}$ in (B12), it is given by

$$N_r^{(n)} = \left(\begin{array}{r} 1 + r^2(n+1)\dfrac{|c_{1n+1}|^2}{|c_{1n}|^2} \\ +r\sqrt{n+1}\left(\dfrac{c_{1n+1}}{c_{1n}} \left\langle \Psi_0^{(n)} | \Psi_1^{(n)} \right\rangle + \left(\dfrac{c_{1n+1}}{c_{1n}} \right)^* \left\langle \Psi_1^{(n)} | \Psi_0^{(n)} \right\rangle \right) \end{array} \right)^{-1/2}. \tag{B15}$$

Thus, the analytical expression for the fidelity Fid_n in (23) is

$$\mathrm{Fid}_n = \left| \left\langle \Psi_n | \Psi_r^{(n)} \right\rangle \right|^2 = N_r^{(n)2} \left(\begin{array}{r} \left| \left\langle \Psi_n | \Psi_0^{(n)} \right\rangle \right|^2 + r\sqrt{n+1} \\ \times \left(\left(\dfrac{c_{1n+1}}{c_{1n}} \right)^* \left\langle \Psi_n | \Psi_0^{(n)} \right\rangle \left\langle \Psi_n | \Psi_1^{(n)} \right\rangle^* + \dfrac{c_{1n+1}}{c_{1n}} \left\langle \Psi_n | \Psi_0^{(n)} \right\rangle^* \left\langle \Psi_n | \Psi_1^{(n)} \right\rangle \right) \end{array} \right), \tag{B16}$$

up to the first order in r.

Appendix C: DV–CV interaction for generation of hybrid entangled states (16)

Consider the following action of two HTBSs

$$\begin{aligned} &BS_{15}BS_{26}\left(|\beta_+\rangle_1 |-\beta_1\rangle_2 |\phi\rangle_{3456} \right) \\ &\quad = N_+ \left(BS_{15}BS_{26}\left(|-\beta\rangle_1 |-\beta_1\rangle_2 |\phi\rangle_{3456} \right) + BS_{15}BS_{26}\left(|\beta\rangle_1 |-\beta_1\rangle_2 |\phi\rangle_{3456} \right) \right). \end{aligned} \tag{C1}$$

Following the steps of calculation as in "Appendix B", we have

$$\begin{aligned} &BS_{15}BS_{26}\left(|-\beta\rangle_1 |-\beta_1\rangle_2 |\phi\rangle_{3456} \right) \\ &\quad = BS_{15}D_1(-\beta)D_5(-\alpha)BS_{15}^+BS_{26}D_2(-\beta_1)D_6(-\alpha_1)BS_{26}^+BS_{15}BS_{26}|00\rangle_{12}D_5(\alpha)D_6(\alpha_1)|\phi\rangle_{3456} \\ &\quad = D_1(-\beta/t)D_5(0)D_2(-\beta_1/t)D_6(0)BS_{15}BS_{26}|00\rangle_{12}(a_0|01\rangle_{34}|0,\alpha\rangle_5|1,\alpha_1\rangle_6 + a_1|10\rangle_{34}|1,\alpha\rangle_5|0,\alpha_1\rangle_6) \end{aligned} \tag{C2}$$

and

$$\begin{aligned} &BS_{15}BS_{26}\left(|\beta\rangle_1 |-\beta_1\rangle_2 |\phi\rangle_{3456} \right) \\ &\quad = BS_{15}D_1(\beta)D_5(\alpha)BS_{15}^+BS_{26}D_2(-\beta_1)D_6(-\alpha_1)BS_{26}^+BS_{15}BS_{26}|00\rangle_{12}D_5(-\alpha)D_6(\alpha_1)|\phi\rangle_{3456} \\ &\quad = D_1(\beta/t)D_5(0)D_2(-\beta_1/t)D_6(0)BS_{15}BS_{26}|00\rangle_{12}(a_0|01\rangle_{34}|0,-\alpha\rangle_5|1,\alpha_1\rangle_6 + a_1|10\rangle_{34}|1,-\alpha\rangle_5|0,\alpha_1\rangle_6). \end{aligned} \tag{C3}$$

Combining the decomposition (A6) with Eqs. (A18) and (A19), we obtain

$$BS_{15}BS_{26}\left(|\beta_+\rangle_1 |-\beta_1\rangle_2 |\phi\rangle_{3456} \right) = N_+F^2 \times \left(\begin{array}{r} |\Delta_0(-\beta,-\beta_1)\rangle_{123456} + |\Delta_0(\beta,-\beta_1)\rangle_{123456} \\ +r\left(|\Delta_1(-\beta,-\beta_1)\rangle_{123456} + |\Delta_1(\beta,-\beta_1)\rangle_{123456} \right) \\ +r^2\left(|\Delta_2(-\beta)\rangle_{123} + |\Delta_2(\beta)\rangle_{123} \right) + \cdots \end{array} \right), \tag{C4}$$

where

$$|\Delta_0(-\beta,-\beta_1)\rangle_{123456}=|-\beta/t\rangle_1|-\beta_1/t\rangle_2\sum_{n=0}^{\infty}\sum_{m=0}^{\infty}c_{0n}(\alpha)c_{1m}(\alpha_1)(a_0|01\rangle_{34}+a_1A_{nm}|10\rangle_{34})|nm\rangle_{56}, \tag{C5}$$

$$|\Delta_0(\beta,-\beta_1)\rangle_{123456}=|\beta/t\rangle_1|-\beta_1/t\rangle_2\sum_{n=0}^{\infty}\sum_{m=0}^{\infty}(-1)^n c_{0n}(\alpha)c_{1m}(\alpha_1)(a_0|01\rangle_{34}-a_1A_{nm}|10\rangle_{34})|nm\rangle_{56}, \tag{C6}$$

$$\begin{aligned}|\Delta_1(-\beta,-\beta_1)\rangle_{123456}&=|1,-\beta/t\rangle_1|-\beta_1/t\rangle_2\sum_{n=1}^{\infty}\sum_{m=0}^{\infty}c_{0n}(\alpha)c_{1m}(\alpha_1)\sqrt{n}t^{n+m-1}(a_0|01\rangle_{34}+a_1A_{nm}|10\rangle_{34})|n-1m\rangle_{56}\\&+|-\beta/t\rangle_1|1,-\beta_1/t\rangle_2\sum_{n=0}^{\infty}\sum_{m=1}^{\infty}c_{0n}(\alpha)c_{1m}(\alpha_1)\sqrt{m}t^{n+m-1}(a_0|01\rangle_{34}+a_1A_{nm}|10\rangle_{34})|nm-1\rangle_{56}\end{aligned} \tag{C7}$$

$$\begin{aligned}|\Delta_1(\beta,-\beta_1)\rangle_{123456}&=|1,\beta/t\rangle_1|-\beta_1/t\rangle_2\sum_{n=1}^{\infty}\sum_{m=0}^{\infty}(-1)^n c_{0n}(\alpha)c_{1m}(\alpha_1)\sqrt{n}t^{n+m-1}(a_0|01\rangle_{34}-a_1A_{nm}|10\rangle_{34})|n-1m\rangle_{56}\\&+|\beta/t\rangle_1|1,-\beta_1/t\rangle_2\sum_{n=0}^{\infty}\sum_{m=1}^{\infty}(-1)^n c_{0n}(\alpha)c_{1m}(\alpha_1)\sqrt{m}t^{n+m-1}(a_0|01\rangle_{34}-a_1A_{nm}|10\rangle_{34})|nm-1\rangle_{56},\end{aligned} \tag{C8}$$

$$\begin{aligned}|\Delta_2(-\beta,-\beta_1)\rangle_{123456}&=|2,-\beta/t\rangle_1|-\beta_1/t\rangle_2\sum_{n=2}^{\infty}\sum_{m=0}^{\infty}c_{0n}(\alpha)c_{1m}(\alpha_1)\sqrt{\frac{n(n-1)}{2!}}t^{n+m-2}\\&(a_0|01\rangle_{34}+a_1A_{nm}|10\rangle_{34})|n-2m\rangle_{56}\\&+|0,-\beta/t\rangle_1|2,-\beta_1/t\rangle_2\sum_{n=0}^{\infty}\sum_{m=1}^{\infty}c_{0n}(\alpha)c_{1m}(\alpha_1)\sqrt{\frac{m(m-1)}{2!}}t^{n+m-2}\\&(a_0|01\rangle_{34}+a_1A_{nm}|10\rangle_{34})|nm-1\rangle_{56}\\&+|1,-\beta/t\rangle_1|1,-\beta_1/t\rangle_2\sum_{n=1}^{\infty}\sum_{m=1}^{\infty}c_{0n}(\alpha)c_{1m}(\alpha_1)\sqrt{nm}t^{n+m-2}\\&(a_0|01\rangle_{34}+a_1A_{nm}|10\rangle_{34})|n-1m-1\rangle_{56},\end{aligned} \tag{C9}$$

$$\begin{aligned}|\Delta_2(\beta,-\beta_1)\rangle_{123456}&=|2,-\beta/t\rangle_1|-\beta_1/t\rangle_2\sum_{n=2}^{\infty}\sum_{m=0}^{\infty}(-1)^n c_{0n}(\alpha)c_{1m}(\alpha_1)\sqrt{\frac{n(n-1)}{2!}}t^{n+m-2}\\&(a_0|01\rangle_{34}-a_1A_{nm}|10\rangle_{34})|n-2m\rangle_{56}\\&+|0,-\beta/t\rangle_{1_1}|2,-\beta_1/t\rangle_2\sum_{n=0}^{\infty}\sum_{m=1}^{\infty}(-1)^n c_{0n}(\alpha)c_{1m}(\alpha_1)\sqrt{\frac{m(m-1)}{2!}}t^{n+m-2}\\&(a_0|01\rangle_{34}-a_1A_{nm}|10\rangle_{34})|nm-1\rangle_{56}\\&+|1,-\beta/t\rangle_1|1,-\beta_1/t\rangle_2\sum_{n=1}^{\infty}\sum_{m=1}^{\infty}(-1)^n c_{0n}(\alpha)c_{1m}(\alpha_1)\sqrt{nm}t^{n+m-2}\\&(a_0|01\rangle_{34}-a_1A_{nm}|10\rangle_{34})|n-1m-1\rangle_{56},\end{aligned} \tag{C10}$$

with

$$A_{nm}(\alpha,\alpha_1)=\frac{c_{1n}(\alpha)c_{0m}(\alpha_1)}{c_{0n}(\alpha)c_{1m}(\alpha_1)}=\frac{\alpha_1\left(n-|\alpha|^2\right)}{\alpha\left(m-|\alpha_1|^2\right)}. \tag{C11}$$

In the limit $t\to 1$ one obtains formula (15) in Sect. 2.2.

References

1. Knill, E., Laflamme, L., Milburn, G.J.: A scheme for efficient quantum computation with linear optics. Nature **409**, 46 (2001)
2. Braunstein, S., van Loock, P.: Quantum information with continuous variables. Rev. Mod. Phys. **77**, 513 (2005)
3. O'Brien, J.L., Furusawa, A., Vučković, J.: Photonic quantum technologies. Nat. Photon. **3**, 687 (2009)
4. Gerry, C.C.: Generation of optical macroscopic quantum superposition states via state reduction with a Mach–Zehnder interferometry containin a Kerr medium. Phys. Rev. A **59**, 4095 (1999)
5. Nielsen, M.A., Chuang, I.L.: Quantum Computation and Quantum Information. University Press, Cambridge (2000)
6. Lutkenhaus, N., Calsamiglia, J., Suominen, K.A.: Bell measurements for teleportation. Phys. Rev. A **59**, 3245 (1999)
7. Bouwmeester, D., Pan, J.W., Mattle, K., Eible, M., Weinfurter, H., Zeilinger, A.: Experimental quantum teleportation. Nature **390**, 575 (1997)
8. Boschi, D., Branca, S., De Martini, F., Harcy, L., Popescu, S.: Experimental realization of teleporting an unknown pure quantum state via dual classical and Einsteing–Podolsky–Rosen channels. Phys. Rev. Lett. **80**, 1121 (1998)
9. Pittman, T.B., Fitch, M.J., Jacobs, B.C., Franson, J.D.: Experimental controlled-NOT logic gate for single photons in the coincidence basis. Phys. Rev. A **68**, 032316 (2003)
10. Braunstein, S.L., Kimble, H.J.: Teleportation of continuous quantum variables. Phys. Rev. Lett. **80**, 869 (1998)
11. Man, Z.X., Xia, Y.J., An, N.B.: Simultaneous observation of particle and wave behaviors of entangled photons. Sci. Rep. **7**, 42539 (2017)
12. Rab, A.S., Polino, E., Man, Z.X., An, N.B., Xia, Y.J., Spagnolo, N., Franco, R.L., Sciarrino, F.: Entanglement of photons in their dual wave-particle nature. Nat. Commun. **8**, 915 (2017)
13. Schrödinger, E.: Die gegenwärtige Situation in der Quantenmechanik. Naturwissenschaften **23**, 807 (1935)
14. van Loock, P., Munro, W.J., Nemoto, K., Spiler, T.P., Ladd, T.D., Braunstein, S.L., Milburn, G.J.: Hybrid quantum computation in quantum optics. Phys. Rev. A **78**, 022303 (2008)
15. Furusava, A., van Loock, P.: Quantum Teleportation and Experiment—A Hybrid Approach to Optical Quantum Information Processing. Wiley-VCH, Weinheim (2011)
16. Lee, S.-W., Jeong, H.: Near-deterministic quantum teleportation and resource-efficient quantum computation using linear optics and hybrid qubit. Phys. Rev. A **87**, 022326 (2013)
17. Podoshvedov, S.A.: Quantum teleportation protocol with assistant who prepares the amplitude modulated unknown qubits. JOSA B **35**, 861 (2018)
18. de Martini, F., Sciarrino, F., Vitelli, C.: Entanglement test on a microscopic–macroscopic system. Phys. Rev. Lett. **100**, 253601 (2008)
19. Morin, O., Haung, K., Liu, J., Jeannic, H.L., Fabre, C., Laurat, J.: Remote creation of hybrid entanglement between particle-like and wave-like optical qubits. Nat. Photonics **8**, 570 (2014)
20. Jeong, H., Zavatta, A., Kang, M., Lee, S.-W., Costanzo, L.S., Grandi, S., Ralph, T.C., Bellini, M.: Generation of hybrid entanglement of light. Nat. Photonics **8**, 564 (2014)
21. Costanzo, L.S., Zavatta, A., Grandi, S., Bellini, M., Jeong, H., Kang, M., Lee, S.-W., Ralph, T.C.: Properties of hybrid entanglement between discrete- and continuous-variable states of light. Phys. Scr. **90**, 074045 (2015)
22. Bich, C.T., Dat, L.T., Hop, N.V., An, N.B.: Deterministic joint remote preparation of an equatorial hybrid state via high-dimensional Einstein–Podolsky–Rosen pairs: active versus passive receiver. Quantum Inf. Process. **17**, 75 (2018)
23. Podoshvedov, S.A.: Generation of displaced squeezed superpositions of coherent states. J. Exp. Theor. Phys. **114**, 451 (2012)
24. Bruno, S., Martin, A., Sekatski, P., Sangouard, N., Thew, R., Gisin, N.: Displacement of entanglement back and forth between the micro and macro domains. Nat. Phys. **9**, 545 (2013)
25. Lvovsky, A.I., Ghobadi, R., Chandra, A., Prasad, A.S., Simon, C.: Observation of micro–macro entanglement of light. Nat. Phys. **9**, 541 (2013)
26. Podoshvedov, S.A.: Elementary quantum gates in different bases. Quant. Inf. Proc. **15**, 3967 (2016)
27. Podoshvedov, S.A.: Building of one-way Hadamard gate for squeezed coherent states. Phys. Rev. A **87**, 012307 (2013)

28. Podoshvedov, S.A., Kim, J., Kim, K.: Elementary quantum gates with Gaussian states. Quantum Inf. Proc. **13**, 1723 (2014)
29. Paris, M.G.A.: Displacement operator by beam splitter. Phys. Lett. A **217**, 78 (1996)
30. Reck, M., Zeilinger, A., Bernstein, H.J., Bertani, P.: Experimental realization of any discrete unitary operator. Phys. Rev. Lett. **73**, 58 (1994)
31. Vidal, G., Werner, R.F.: Computable measure of entanglement. Phys. Rev. A **65**, 032314 (2002)
32. Peres, A.: Separability criterion for density matrices. Phys. Rev. Lett. **77**, 1413 (1996)
33. Wootters, W.K.: Entanglement of formation of an arbitrary state of two qubits. Phys. Rev. Lett. **80**, 2245 (1998)
34. An, N.B.: Teleportation of coherent state superposition within a network. Phys. Rev. A **68**, 022321 (2003)
35. Shanta, P., Chaturverdi, S., Srinivasan, V., Agarwal, G.S., Mehta, C.L.: Unified approach to multiphoton coherent states. Phys. Rev. Lett. **72**, 1447 (1994)
36. Laha, P., Lakshmibala, S., Balakrishnan, V.: Estimation of nonclassical properties of multiphoton coherent states from optical tomograms. J. Mod. Optics (2018). https://doi.org/10.1080/09500340.2018.1454527